



Contents lists available at ScienceDirect



## Catalysis Today

journal homepage: [www.elsevier.com/locate/cattod](http://www.elsevier.com/locate/cattod)

# Esterification of levulinic acid with ethanol over sulfated mesoporous zirconosilicates: Influences of the preparation conditions on the structural properties and catalytic performances

Yasutaka Kuwahara <sup>a,\*</sup>, Tadahiro Fujitani <sup>a</sup>, Hiromi Yamashita <sup>b</sup>

<sup>a</sup> Research Institute for Innovation in Sustainable Chemistry, National Institute of Advanced Industrial Science and Technology (AIST), 1-1-1 Higashi, Tsukuba, Ibaraki 305-8565, Japan

<sup>b</sup> Division of Materials and Manufacturing Science, Graduate School of Engineering, Osaka University, 2-1 Yamadaoka, Suita, Osaka 565-0871, Japan

## ARTICLE INFO

### Article history:

Received 1 August 2013

Received in revised form 30 October 2013

Accepted 14 November 2013

Available online xxx

### Keywords:

Biomass conversion

Levulinic acid

Esterification

Solid acid catalyst

Mesoporous zirconosilicate

## ABSTRACT

Levulinic acid is considered one of the most important biomass-derived chemicals owing to its potential as a versatile building block to synthesize valuable fuels and chemicals. Levulinate esters, such as methyl levulinate and ethyl levulinate obtained via esterification of levulinic acid with alcohols, can in particular be used as fuel additives and plasticizers, and thus have a potential to replace a significant amount of petroleum-derived chemical feedstocks. In this article, sulfated zirconosilicates having P6mm hexagonal mesoporous structure were applied as solid acid catalysts to the esterification of levulinic acid with ethanol to produce ethyl levulinate, and the influences of preparation conditions on the structural properties and catalytic performances were investigated. A distinct correlation was observed between the catalytic activity and the density of acid sites, showing that dispersibility of the acid sites and the associated accessibility of the organic reactants play an important role in determining the overall activity. Among the catalysts tested, sulfated Zr-SBA-15 with optimum Zr content (Si/Zr ratio of 10.7) was found to be the best catalyst, the activity of which was far superior to that of conventional sulfated  $ZrO_2$ . In addition, direct conversion of cellulosic sugars (glucose and fructose) into levulinate esters was also examined.

© 2013 Elsevier B.V. All rights reserved.

## 1. Introduction

Driven by increasing concern over the depletion of petroleum resources, use of biomass as renewable natural resources and its conversion into valuable biofuels and feedstock chemicals have received considerable attention in recent years [1–4]. Among various chemicals synthesized from cellulose and cellulosic biomass, levulinic acid (LA) and its esters are gaining increasing attention as promising platform chemicals for a range of derivatives in the biofuel, polymer and specialty chemicals markets [5–10]. LA is a molecule generally produced by the acid-catalyzed hydrolysis of cellulose [11–13], and can catalytically be converted into levulinate esters [10,14–16],  $\gamma$ -valerolactone [5–7,17–20], 1,4-pentanediol [5] and 5-nonenone (via pentanoic acid) [21] as well as diphenolic acid as an intermediate for the synthesis of epoxy resins and polycarbonates [22,23]. Levulinate esters are also useful compounds that can be used as fuel additives, solvents and plasticizers. In particular, ethyl levulinate can directly be used up to 5 wt% as a diesel

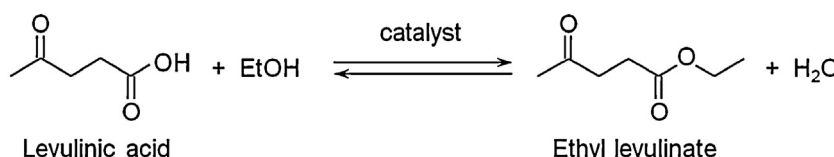
miscible biofuel in regular diesel car engines without modification owing to their physicochemical properties similar to the biodiesel fatty acid methyl esters (FAME), and thus has a potential to reduce the consumption of petroleum-derived fossil fuels [10,16].

Generally, levulinate esters are produced by esterification of LA with several alcohols using mineral acids such as  $HCl$ ,  $H_2SO_4$  and  $H_3PO_4$  (Scheme 1), which leads to a high yield of corresponding products within a short reaction period. However, such homogeneous acid catalysts are unrecyclable and always suffer from operational problems (e.g., use of a large volume of base for neutralization and corrosion of equipment). Therefore, substitution of homogeneous catalysts by heterogeneous analogues that are easily separable and reusable over repeated cycles is highly desirable.

Several kinds of solid acid catalysts have been reported so far for the esterification of LA with alcohols. Baronetti et al. examined the esterification of LA with ethanol at 78 °C using silica-stabilized Wells–Dawson heteropolyacids [14]. Bokade et al. used montmorillonite-supported heteropolyacids for the esterification of LA with *n*-butanol to obtain *n*-butyl levulinate at 120 °C [15]. These precedent works indicate that LA can be transformed to levulinate esters in excellent yields over solid acid catalysts which possess as strong acid strength as that of heteropolyacids.

\* Corresponding author. Tel.: +81 29 861 2790.

E-mail address: [y.kuwahara@aist.go.jp](mailto:y.kuwahara@aist.go.jp) (Y. Kuwahara).



**Scheme 1.** Esterification of levulinic acid with ethano

Recently, Silva et al. screened several types of solid acid catalysts (e.g., zeolites and sulfated mixed oxides) through the esterification of LA with ethanol and found that sulfated mixed oxides (sulfated zirconia ( $\text{SO}_4^{2-}/\text{ZrO}_2$ ), niobia ( $\text{SO}_4^{2-}/\text{Nb}_2\text{O}_5$ ), titania ( $\text{SO}_4^{2-}/\text{TiO}_2$ ) and stannia ( $\text{SO}_4^{2-}/\text{SnO}_2$ )) bearing a number of strong acid sites are the most promising candidates providing high catalytic activity within an appropriate period of time [16]. Nevertheless, the reaction rates are likely dependent on the number of acid sites and the preparation conditions applied, still leaving room for a further study; there might be a possibility that the activity of sulfated mixed oxides for this reaction can further be improved by optimizing preparation conditions, the number of acid sites and dispersion state of the sulfate species by introducing more elaborated catalyst preparation techniques. One possible approach is the introductions of mesopores in the mixed oxides via a surfactant-induced self-assembly approach. Mesoporosity is especially effective in liquid-state catalysis for easy transport of the reactant molecules and the resulting high surface area provides better dispersion of the acid sites and an increased number of acid sites [24,25].

Herein, we report the esterification of levulinic acid with ethanol to produce ethyl levulinate over sulfated mesoporous zirconosilicate materials. Among a number of choices of mesoporous silicate structure, SBA-15 type structure consisting of two-dimensional cylindrical pores arranged in a hexagonal order ( $P6mm$  symmetry) was chosen, because of its pore diameter larger than that of MCM-41 analogues. Larger pore diameter provides a wider space for mass transportation, which may allow reactants to more efficiently access to the active sites dispersed inside the pore channels. A series of sulfated zirconosilicates having  $P6mm$  hexagonal mesoporous structure with varied Zr content were synthesized by sol-gel process using Pluronic P123 block copolymer as a pore-directing agent and tetraethylorthosilicate as a silicon source either via a post-sulfation or via a direct-sulfation procedure. The influences of preparation conditions and Zr content on structural properties and catalytic performances were investigated in detail. The activities of the catalysts were examined by the esterification of LA with ethanol at  $70^{\circ}\text{C}$  and were compared with that of the conventional sulfated zirconia. Furthermore, conversions of cellulosic sugars (glucose and fructose) directly into levulinate esters by acid-catalyzed thermolysis in methanol were also examined using a few selected samples.

## 2. Experimental

### **2.1. Preparation of sulfated mesoporous zirconosilicate via a post-sulfation procedure**

The typical synthetic procedure for the post-sulfation route is as follows [26–28]. An amount of 3.0 g of Pluronic P123 ( $\text{PEO}_{20}\text{-PPO}_{70}\text{-PEO}_{20}$ , Aldrich,  $M_W = 5800$ ) and 1.77 g of NaCl was dissolved in 120 mL of deionized water with vigorous stirring for 2 h in a flask. To this micellar solution, a designated amount of zirconium oxychloride octahydrate ( $\text{ZrOCl}_2\cdot 8\text{H}_2\text{O}$ , Aldrich, >99%) and 6.44 g of tetraethylorthosilicate (TEOS, Wako Pure Chemical Industries, 95%) were sequentially added and stirred at 40 °C for 1 day. The molar ratio of the initial gel was adjusted to P123: Si: Zr: NaCl:  $\text{H}_2\text{O} = 0.017$ : 1.0: (0–0.2): 1.0: 220. The solution was then transferred to a pressure bottle, sealed, and hydrothermally treated at

100 °C for another day under static conditions. The resulting product was filtered, washed with deionized water, dried overnight and finally calcined in air at 600 °C for 6 h to remove the organic template. The thus obtained solids were subsequently sulfated by suspending 2.0 g of solid in 30 mL of 1.0 M of sulfuric acid solutions for 1 h, followed by vacuum filtration, drying at 100 °C overnight and calcination in air at 600 °C for 3 h. The obtained samples were denoted as S-ZrSBA15( $X$ ), where  $X$  is the atomic ratio of Si/Zr in the final solid.

For comparison, a pure siliceous SBA-15 sample was prepared the same way as the above procedure except for the addition of zirconium source. A sulfated zirconia ( $\text{SO}_4^{2-}/\text{ZrO}_2$ ) was also prepared by the conventional wet impregnation method [29,30]; a total of 5.8 g of  $\text{ZrOCl}_2 \cdot 8\text{H}_2\text{O}$  was dissolved in 200 mL of deionized water, followed by precipitation of zirconium hydroxide at pH 9.0 using 10%  $\text{NH}_3$  solution, aging at room temperature for 2 days and calcination in air at 600 °C for 3 h. The resulting  $\text{ZrO}_2$  was then suspended in 1.0 M of sulfuric acid solutions (15 mL per gram of solid) for 1 h, followed by vacuum filtration, drying at 100 °C overnight and calcination in air at 600 °C for 3 h.

## *2.2. Preparation of sulfated mesoporous zirconosilicate via a direct-sulfation procedure*

Sulfated mesoporous zirconosilicates with larger Zr contents were also synthesized via a direct-sulfation route according to the methods previously reported by Mou et al. [24]. In a typical synthesis, 3.0 g of Pluronic P123 was dissolved in 100 mL of HCl aqueous solution with vigorous stirring for 2 h in a flask. To this micellar solution, an amount of ammonium sulfate ( $(\text{NH}_4)_2\text{SO}_4$ , Wako Pure Chemical Industries, 99.5%) and a mixture solution of TEOS and zirconium tetrapropoxide ( $\text{Zr}(\text{O}^n\text{Pr})_4$ , Aldrich, 70% w/w in 1-propanol) were sequentially added and stirred at 40 °C for 1 day. The molar ratio of the initial gel was adjusted to P123: Si: Zr: HCl:  $\text{H}_2\text{O} = 0.017: 1.0: (0.25-1.0): 4.7: 180$ , and the  $\text{SO}_4^{2-}/\text{Zr}$  molar ratio was fixed to 1.0. The solution was transferred to an oven and then hydrothermally reacted at 100 °C for another day under static conditions. The resulting product was filtered, washed with deionized water, dried overnight at 100 °C, and finally calcined at 600 °C for 6 h to remove the organic template. The synthesized samples were named as S-mesoZS( $X$ ), where  $X$  is the atomic ratio of Si/Zr in the final solid.

### 2.3. Characterization

Powder X-ray diffraction (XRD) patterns were collected using a Bruker AXS D8 Advance X-ray diffractometer equipped with a scintillation counter for low-angle region and a LynxEye detector for high-angle region with CuK $\alpha$  radiation ( $\lambda = 1.54056 \text{ \AA}$ ). Scans were performed at step size 0.02° over the 2 $\theta$  range of 0.5–80°. Nitrogen adsorption–desorption isotherms were measured at -196 °C by using Micromeritics ASAP2020. The samples were degassed at 300 °C under vacuum for 4 h prior to the measurements to vaporize physisorbed water. The specific surface area was calculated by the BET (Brunauer–Emmett–Teller) method by using adsorption data ranging from  $P/P_0 = 0.05$  to 0.30. The pore size distributions were obtained from the adsorption branch of the nitrogen isotherms by

the BJH (Barret–Joyner–Halenda) method. Infrared spectra were recorded with a JASCO FTIR-6300 instrument in the spectral range 2000–400 cm<sup>-1</sup> under vacuum with a resolution of 4 cm<sup>-1</sup> using samples diluted with KBr. Diffuse reflectance UV-vis spectra were collected using a Shimadzu UV-2600 spectrophotometer equipped with an integrating sphere in the spectral range of 200–400 nm. Absorption spectra were calculated using the Kubelka–Munk function. Inductively coupled plasma atomic emission spectrometry (ICP-AES) was used to quantify sulfur contents in the samples.

The acidity of catalysts was studied by temperature programmed desorption of NH<sub>3</sub> (NH<sub>3</sub>-TPD) by using a BELCAT-B system (BEL Japan, Inc.). Approximately 100 mg of each sample was preheated under a He flow (50 mL/min) at 600 °C for 1 h, allowed to cool to 50 °C, and subsequently exposed to flowing 5% NH<sub>3</sub>/He gas mixture (50 mL/min) for 1 h. Then, the system was purged at 50 °C for 0.5 h with He to eliminate weakly adsorbed NH<sub>3</sub>. NH<sub>3</sub>-TPD was carried out between 50 and 600 °C under a He flow (30 mL/min) with a ramping rate of 10 °C/min, and the desorbed NH<sub>3</sub> was quantified by an on-line thermal conductivity detector.

#### 2.4. Esterification of levulinic acid with ethanol

Levulinic acid esterification was carried out in a quartz glass reactor with a reflux condenser. The reactions were typically performed at 70 °C for up to 24 h under stirring of 700 rpm using 5.0 wt% of solid acid catalysts and with the molar ratio of LA:EtOH = 1:10. A portion of the reaction mixture was withdrawn at appropriate intervals, filtered and analyzed by using a gas chromatography (GC; Shimadzu GC-14B) with a flame ionization detector equipped with a capillary column (ULBON HR-20 M; 0.53 mm × 30 m; Shinwa Chemical). The levulinic acid conversion (or ethyl levulinate yield) was calculated based on the levulinic acid/ethyl levulinate area ratio. To examine the catalyst recyclability, the spent catalyst was recovered from the reaction solution by simple filtration, washed with acetone, calcined at 600 °C in air for 3 h to remove the strongly adsorbed organic species and then subjected to next catalytic run.

#### 2.5. Direct conversion of cellulosic sugars into methyl levulinate

Direct conversion of sugars (either glucose or fructose) into methyl levulinate was performed in a 60 mL cylindrical stainless steel autoclave reactor (EYELA, Inc.) [31]. 450 mg of sugars (Aldrich, 2.5 mmol), 20 mL of methanol (Aldrich, reagent grade) and 2.5 wt% of catalyst were introduced into the reactor, which was then sealed, purged and pressurized with 0.5 MPa of N<sub>2</sub> and heated at 200 °C for 3 h with magnetic stirring. After cooling, the reaction mixture was filtered and analyzed with a high performance liquid chromatography (HPLC; Shimadzu). The yields of products and unreacted sugars were quantified by an internal standard method.

### 3. Results and discussion

#### 3.1. Structural analysis

The structural characteristics of a series of sulfated mesoporous zirconosilicates were investigated by XRD measurement and N<sub>2</sub> physisorption. Fig. 1 shows XRD patterns of S-ZrSBA15 with varied Si/Zr atomic ratios (corresponding to 0.38–17.8 mol% Zr/Si). The Si/Zr atomic ratio in the final solids were higher than the ones in the initial gel solutions (see Table 1), indicating that some fraction of Zr species remained unincorporated into the silicate particles under the synthesis conditions applied in this study. Low angle XRD patterns of S-ZrSBA15 with the Si/Zr atomic ratio above 15.5 exhibited defined single peaks at around 2θ = 0.8–0.9° and two adjacent small

**Table 1**  
Textural properties of sulfated mesoporous zirconosilicate materials.

Sample	Si/Zr <sup>a</sup>		Sulfur content <sup>a</sup> (wt%)		XRD d-Spacing <sup>b</sup> (nm)		N <sub>2</sub> physisorption		
	Initial gel	Product	Initial gel	Product	Lattice parameter <i>a</i> <sup>c</sup> (nm)	S <sub>BET</sub> <sup>d</sup> (m <sup>2</sup> /g)	<i>V</i> <sub>total</sub> <sup>e</sup> (cm <sup>3</sup> /g)	<i>D</i> <sub>p</sub> <sup>f</sup> (nm)	
Unmodified SBA-15	∞	∞	—	—	9.9	14.0	848	1.56	9.9
S-ZrSBA15(26.6)	20.0	26.6	—	0.47	9.9	14.0	585	0.88	8.9
S-ZrSBA15(15.5)	10.0	15.5	—	0.43	0.95	10.0	524	0.76	8.7
S-ZrSBA15(10.7)	6.7	10.7	—	0.32	0.97	10.3	515	0.56	5.0
S-ZrSBA15(5.6)	5.0	5.6	—	0.19	0.98	11.8	454	0.36	2.2
S-mesoZS(7.9)	4.0	7.9	1.0	0.043	0.14	10.3	695	1.25	11.0
S-mesoZS(6.6)	3.0	6.6	1.0	0.069	0.28	9.9	642	1.23	10.6
S-mesoZS(3.7)	2.0	3.7	1.0	0.056	0.33	9.3	555	1.05	9.7
S-mesoZS(1.7)	1.0	1.7	1.0	0.039	0.37	9.3	392	0.72	9.7

<sup>a</sup> Molar ratio determined by the combination of ICP and EDX analyses.

<sup>b</sup> Calculated from Bragg equation:  $2d \sin \theta = n\lambda$  ( $\lambda = 0.1541$  nm).

<sup>c</sup> Defined by  $a_0 = 2d_{100}/\sqrt{3}$  assuming hexagonal structure.

<sup>d</sup> Specific surface area calculated by BET method from N<sub>2</sub> adsorption data ranging from  $P/P_0 = 0.05$  to 0.30.

<sup>e</sup> Total pore volume at  $P/P_0 = 0.99$ .

<sup>f</sup> Average pore diameter determined by BJH method.

<sup>g</sup> Wall thickness defined by  $T_w = a_0 - D_p$ .

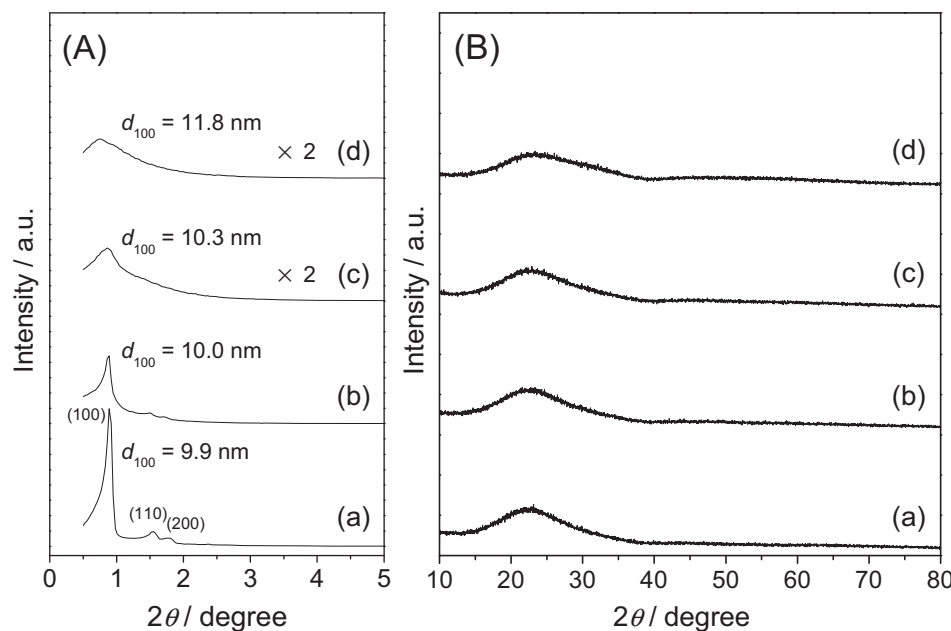


**Fig. 1.** (A) Small-angle and (B) wide-angle XRD patterns of S-ZrSBA15 with varied Si/Zr atomic ratios (Si/Zr = (a) 26.6, (b) 15.5, (c) 10.7, and (d) 5.6 in the final solid). Several diffraction planes associated with 2D hexagonal mesoporous structure ( $P6mm$ ) are indicated for S-ZrSBA15(26.6).

diffractions that are assigned to the (1 0 0), (1 1 0) and (2 0 0) reflections, respectively, showing that these samples have 2D hexagonal mesoporous structures with  $P6mm$  symmetry (Fig. 1A(a) and (b)). On the other hand, S-ZrSBA15 with the Si/Zr atomic ratio below 10.7 exhibited less resolved, broad diffraction peaks in this region, suggesting a decrease in the ordered pore arrangement for these samples.

This disordered arrangement of mesopores can be elucidated by nitrogen adsorption isotherms. S-ZrSBA15(26.6) displayed a type IV isotherm with clear capillary condensation at around  $P/P_0 = 0.7$ , reflecting the presence of defined mesopore channels with narrow pore size distributions (Fig. 2A(a)). The adsorbed nitrogen quantities appreciably decreased and the hysteresis in the isotherms gradually disappeared as the Zr content increased (Fig. 2A(b)–(d)).

The textural parameters obtained from XRD measurement and N<sub>2</sub> adsorption isotherms are summarized in Table 1. Along with the decrease in the Si/Zr ratio from 26.6 to 5.6, the specific surface areas and total pore volumes decreased from 585 to 454 m<sup>2</sup>/g and 0.88 to 0.36 cm<sup>3</sup>/g, respectively. The pore size distribution curves calculated by the BJH method show that the average pore diameter decreased from 8.9 to 2.2 nm (Fig. 2B), being coincided with the increases in d-spacing values and the corresponding lattice parameter  $a_0$  (pore to pore distance) as well as pore wall thickness  $T_w$  calculated from XRD data. These combined results reveal that the ordered structure of SBA-15 silica appears to degrade at higher percentages of Zr (more than 5.0 mol% per Si), and accordingly results in reduced mesoporosity [25–28,32–34]. Nonetheless, the materials still had large surface areas and pore volumes as to be regarded

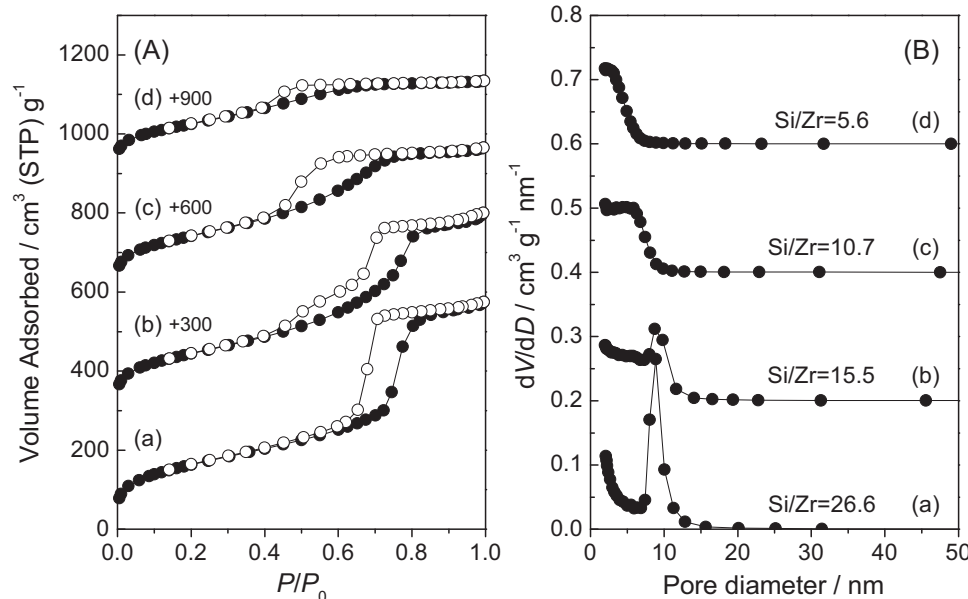


**Fig. 2.** (A) Nitrogen adsorption–desorption isotherms and (B) the corresponding pore size distribution curves of S-ZrSBA15 with varied Si/Zr atomic ratios (Si/Zr = (a) 26.6, (b) 15.5, (c) 10.7 and (d) 5.6 in the final solid). Filled and empty symbols in the left represent adsorption and desorption branches, respectively.

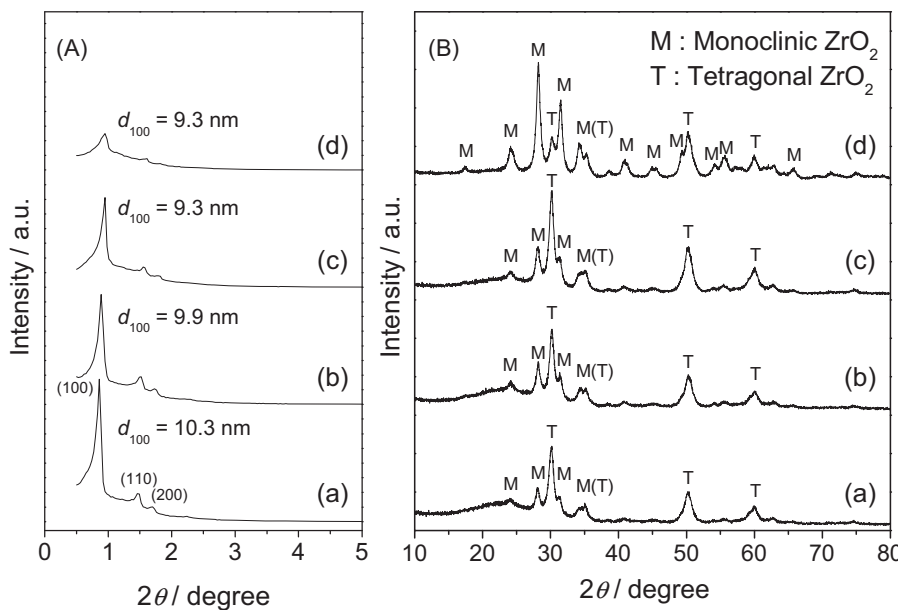


**Fig. 3.** (A) Small-angle and (B) wide-angle XRD patterns of S-mesoZS with varied Si/Zr atomic ratios (Si/Zr = (a) 7.9, (b) 6.6, (c) 3.7 and (d) 1.7 in the final solid). Several diffraction planes associated with 2D hexagonal mesoporous structure ( $P6mm$ ) are indicated for S-mesoZS(7.9), and diffraction planes assigned to monoclinic (M) and tetragonal (T)  $ZrO_2$  crystals are indicated in the right.

as mesoporous materials. In high angle XRD patterns, no crystalline phase could be observed at all Zr loading levels, except for broad peaks attributable to amorphous silicate phase, suggesting an iso-morphous substitution of Zr atoms within the silica matrix in the S-ZrSBA15 samples [28,33,34].

Fig. 3 shows XRD patterns of S-mesoZS with varied Si/Zr atomic ratios (corresponding to 12.7–58.8 mol% Zr/Si). While S-mesoZS materials contain much higher Zr contents than S-ZrSBA15 materials, they exhibited well-defined diffraction planes associated with 2D hexagonal mesoporous structure ( $P6mm$ ) in all Zr loading levels (Fig. 3A). In  $N_2$  adsorption, a series of S-mesoZS materials showed typical type IV isotherms with clear inflections at around  $P/P_0 = 0.7$  and with narrow pore size distributions centered at around 10 nm (Fig. 4). The specific surface areas and total pore volumes decreased from 695 to 392  $m^2/g$  and 1.25 to 0.72  $cm^3/g$ , respectively, as the

Si/Zr ratio decreased from 7.9 to 1.7; however, the pore-associated parameters, such as d-spacing value, average pore diameter and wall thickness, scarcely changed, indicating a retention of the ordered mesoporous structure. It should be noted that a series of S-mesoZS materials have relatively larger pore volumes and wider pore channels compared to those of S-ZrSBA15 materials, despite the incorporation of larger Zr content.

The most obvious difference between S-mesoZS and S-ZrSBA15 samples was observed in their crystalline structure. In high angle XRD patterns, S-mesoZS samples exhibited diffraction planes associated with both monoclinic  $ZrO_2$  ( $2\theta = 24.2, 28.2, 31.4$  and  $34.4^\circ$ ) and tetragonal  $ZrO_2$  ( $2\theta = 30.2, 49.6, 50.4$  and  $60.1^\circ$ ) (Fig. 3B), evidencing the aggregation of Zr species. This difference in the crystalline phase is due to the different zirconium precursors used ( $ZrOCl_2 \cdot 8H_2O$  for S-ZrSBA15 and  $Zr(O^{\prime}Pr)_4$  for S-mesoZS) and the

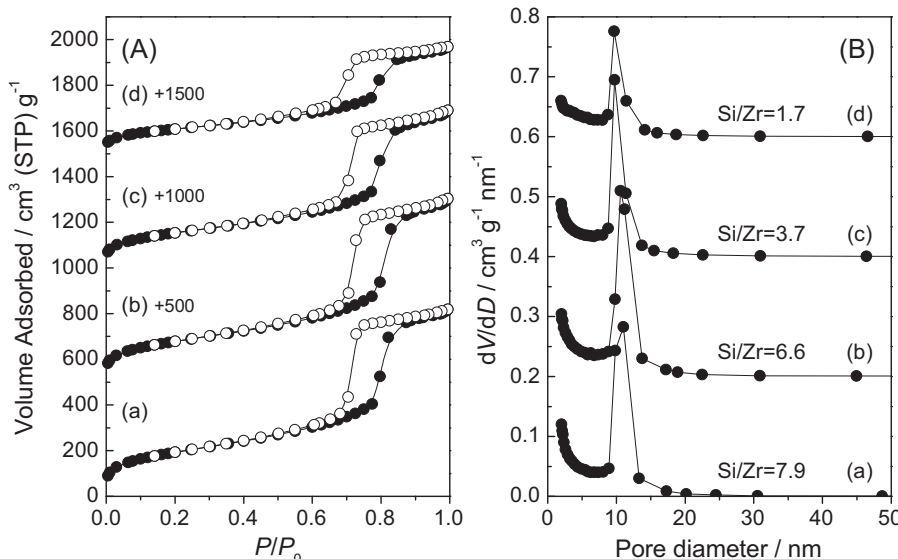


**Fig. 4.** (A) Nitrogen adsorption–desorption isotherms and (B) the corresponding pore size distribution curves of S-mesoZS with varied Si/Zr atomic ratios (Si/Zr = (a) 7.9, (b) 6.6, (c) 3.7 and (d) 1.7 in the final solid). Filled and empty symbols in the left represent adsorption and desorption branches, respectively.

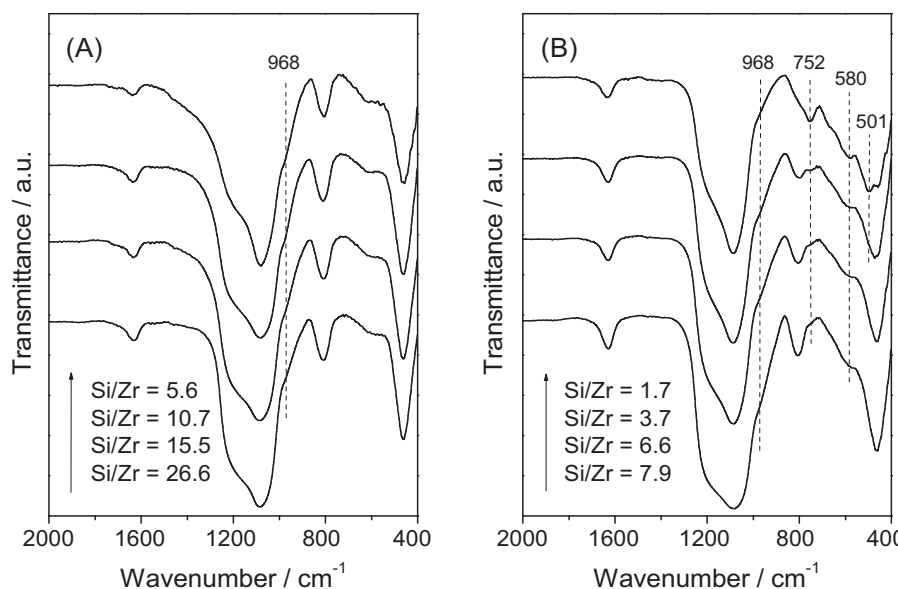


**Fig. 5.** FTIR spectra of (A) S-ZrSBA15 samples and (B) S-mesoZS samples with different Si/Zr atomic ratios.

different synthetic conditions applied (almost neutral condition for S-ZrSBA15 and strong acidic condition for S-mesoZS). Considering the fact that the adsorption–desorption branches were essentially parallel and the average pore diameter scarcely changed, most Zr species in the S-mesoZS materials are likely to be present inside the mesoporous silica wall as nano-crystalline ZrO<sub>2</sub> particles without significant pore blocking (extra-framework aggregated ZrO<sub>2</sub> particles were not observed in the TEM images).

### 3.2. Investigation of chemical environment of Zr species

In order to verify the chemical environment of the incorporated Zr atoms, the samples were characterized with FTIR and UV-vis techniques. Usually, pure siliceous mesoporous silica shows several infrared absorption bands at around 460, 806, 1085, 1235, 1630 cm<sup>-1</sup>. The band at 1630 cm<sup>-1</sup> is associated with O–H bending vibration of adsorbed H<sub>2</sub>O molecules and surface silanol

groups [32,35]. The bands at 460, 806, 1085 cm<sup>-1</sup> are assigned to the bending, symmetric stretching and asymmetric stretching vibration of the Si–O–Si bond, respectively [32,35]. The intensity of the band positioned at around 968 cm<sup>-1</sup> can be a good indicator of the formation of the Si–O–Zr bond [32]. In the case of S-ZrSBA15 samples, the intensity of this band quantitatively increased as the Zr content in the samples increased (Fig. 5A), indicating the incorporation of larger Zr atoms into the silica framework. Contrary to this, in the IR spectra of the S-mesoZS samples, the intensity of the band at 968 cm<sup>-1</sup> gradually diminished as increasing the Zr content, simultaneously with which specific bands assignable to contiguous Zr–O–Zr bond appeared at 501, 580, 752 cm<sup>-1</sup> (Fig. 5B), indicating the formation of aggregated ZrO<sub>2</sub> species at high Zr loading levels [35]. It should be noted that no appreciable difference was observed in higher wavenumber region of the IR spectra, in which only a broad band corresponding to the O–H stretching

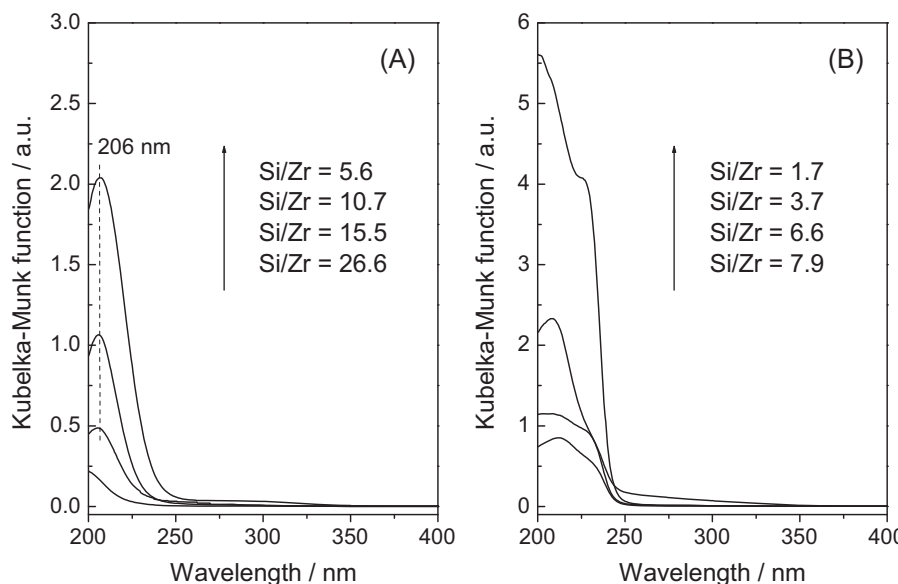


**Fig. 6.** Diffuse reflectance UV-vis spectra of (A) S-ZrSBA15 samples and (B) S-mesoZS samples with different Si/Zr atomic ratios.

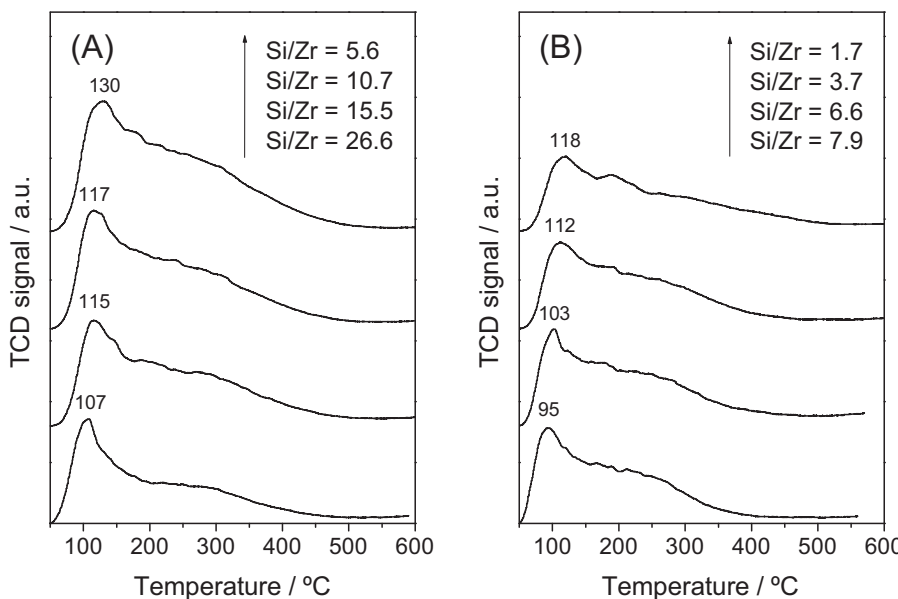


**Fig. 7.** NH<sub>3</sub>-TPD profiles of (A) S-ZrSBA15 samples and (B) S-mesoZS samples with different Si/Zr atomic ratios. TCD signals were normalized by the weight of the samples used in each experiment.

vibration associated with physisorbed H<sub>2</sub>O molecules and Si-OH (or Zr-OH) terminal groups was observed in all the samples.

The above result has been corroborated by UV-vis measurement (Fig. 6). In the diffuse reflectance UV-vis spectra, the S-ZrSBA15 samples showed sole absorption bands at 206 nm. This band is attributed to the presence of monomeric Zr atoms surrounded by four oxygen-bridged Si atoms, revealing that the incorporated Zr atoms are dominantly present as monodispersed Zr atoms within the silica matrix [24,27,28]. On the contrary, the S-mesoZS samples exhibited absorption bands extended towards longer wavelength region (~245 nm). This is the absorption band typical of bulk ZrO<sub>2</sub> [24,27,28], proving that Zr in the S-mesoZS samples are mainly present in the form of crystalline ZrO<sub>2</sub> (possibly containing monomeric/polymeric zirconium oxide moieties as well, due to the presence of specific absorption at 200–220 nm).

Thus, the coordination geometry of the incorporated Zr atoms, as well as the resulting quality of mesoporous structure, alter depending on the kind and amount of the Zr precursors used and the synthetic conditions applied; synthesis by using zirconium oxychloride and under mild conditions afforded mesoporous zirconosilicates having monodispersed Zr within the silica matrix, and

on the other hand, synthesis by using zirconium alkoxide precursor and under strong acid conditions yielded high-quality mesoporous zirconosilicates with larger Zr contents embedding crystalline ZrO<sub>2</sub> particles inside their silica walls.

### 3.3. Acidity measurement

The acidity of the catalysts that substantially affects their catalytic performances was investigated by TPD measurement using NH<sub>3</sub> as a probe molecule. Normalized NH<sub>3</sub>-TPD profiles of S-ZrSBA15 and S-mesoZS samples are shown in Fig. 7A and B, respectively. All samples exhibited desorption peaks positioned at 100–130 °C which are assigned to weak acid sites and desorption peaks distributed in the range of 150–400 °C which correspond to medium acid sites. In the case of S-ZrSBA15 samples, the intensity of desorption peak was enhanced and the desorption peak was slightly shifted to higher temperature region (from 107 to 130 °C) in accordance with the decrease in the Si/Zr atomic ratio from 26.6 to 5.6. As summarized in Table 2, a quantitative analysis demonstrated that a higher sulfur content was provided by S-ZrSBA15 having larger Zr content, and accordingly led to an increased amount of acid sites. Similarly, S-mesoZS also provided a higher sulfur content

**Table 2**

Textural properties of sulfated mesoporous zirconosilicate materials.

Sample	Sulfur content <sup>a</sup> (wt%)	Acidity		Catalytic activity <sup>d</sup> (%)
		Acid amount <sup>b</sup> (mmol/g)	Acid density <sup>c</sup> (μmol/m <sup>2</sup> )	
Unmodified SBA-15	–	0.172	0.20	6.2
S-ZrSBA15(26.6)	0.58	0.567	0.97	58.3
S-ZrSBA15(15.5)	0.95	0.689	1.31	66.2
S-ZrSBA15(10.7)	0.97	0.810	1.57	79.0
S-ZrSBA15(5.6)	0.98	0.935	2.06	68.5
S-mesoZS(7.9)	0.14	0.631	0.91	43.8
S-mesoZS(6.6)	0.28	0.632	0.98	49.6
S-mesoZS(3.7)	0.33	0.594	1.07	59.6
S-mesoZS(1.7)	0.37	0.527	1.34	63.3
SO <sub>4</sub> <sup>2-</sup> /ZrO <sub>2</sub>	0.60	0.534	10.27	31.8

<sup>a</sup> Determined by the combination of ICP and EDX analyses.

<sup>b</sup> Amount of NH<sub>3</sub> chemisorbed per gram of sample.

<sup>c</sup> Calculated by the equation: [acid density (μmol/m<sup>2</sup>)]=[acid amount (mmol/g)]/[specific surface area of sample (m<sup>2</sup>/g)] × 1000.

<sup>d</sup> Yield of ethyl levulinate after 24 h of reaction under the standard reaction conditions (5.0 wt% of catalyst, LA:EtOH = 1:10, 70 °C, 700 rpm).

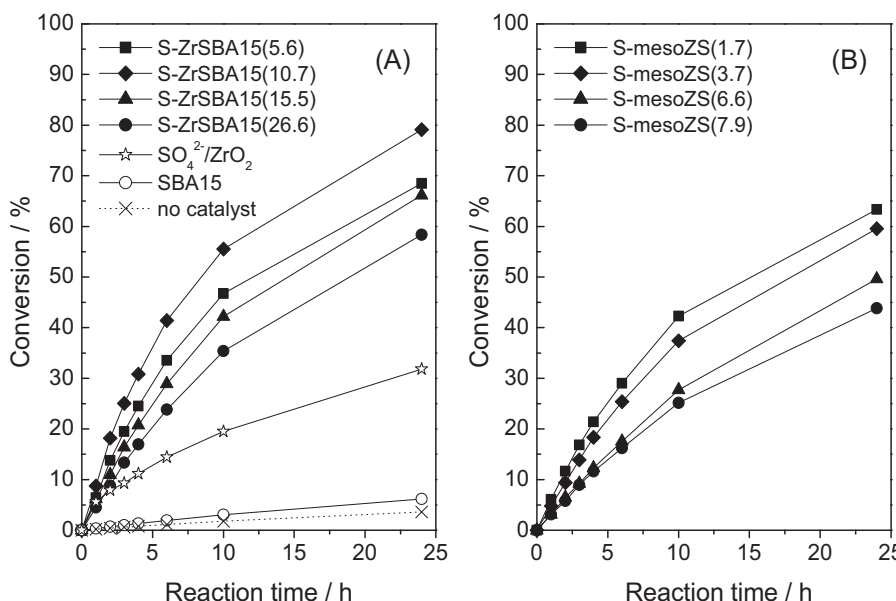


**Fig. 8.** Esterification of levulinic acid with ethanol over sulfated mesoporous zirconosilicate catalysts: (A) S-ZrSBA15 with varied Si/Zr atomic ratios, sulfated zirconia ( $\text{SO}_4^{2-}/\text{ZrO}_2$ ), unmodified SBA-15 and without catalyst. (B) S-mesoZS with varied Si/Zr atomic ratios. Reaction conditions: 5.0 wt% of catalyst, LA:EtOH = 1:10, 70 °C, 700 rpm.

as increasing the Zr content in the samples; however, the sulfur contents of S-mesoZS samples were overall smaller than those found in S-ZrSBA15 samples, indicating that  $\text{SO}_4^{2-}$ -species are more easily attached on zirconia via a post-sulfation route. It is also interesting that, in the S-mesoZS samples, the total amount of acid sites decreased as opposed to the increase in the Zr (and sulfur) content (see Table 2). This result clearly indicates that some fraction of sulfate anions ( $\text{SO}_4^{2-}$ ) in the S-mesoZS samples are inaccessible by  $\text{NH}_3$  molecules probably due to the existence of intra-framework  $\text{SO}_4^{2-}$  species, while those attached on the S-ZrSBA15 samples are most likely surface-exposed and accessible for reactant molecules. This difference is probably the consequence of the different preparation method applied (i.e., post- and direct-sulfation procedure).

### 3.4. Esterification of levulinic acid with ethanol over sulfated mesoporous zirconosilicates

The esterification of levulinic acid with ethanol was carried out at 70 °C using 5.0 wt% of catalyst and with LA:EtOH = 1:10 over the sulfated mesoporous zirconosilicates, sulfated zirconia and

unmodified SBA-15 materials. The reaction profiles are shown in Fig. 8, and the yields of ethyl levulinate after 24 h of the reaction are listed in Table 2.

The esterification of levulinic acid with alcohols proceeds even in absence of catalyst, because LA itself shows strong acidity capable of catalyzing the reaction [16]; a blank experiment demonstrated that 3.6% of ethyl levulinate can be yielded in the absence of catalyst at 70 °C after 24 h of reaction. Unmodified SBA-15 gave an absolutely low yield of ethyl levulinate (6.2%) after 24 h of reaction, although it is slightly higher than that in the blank experiment. As shown in Fig. 8, the reaction was significantly accelerated in the presence of the solid acid catalysts. When a series of sulfated Zr-SBA15 were used as catalysts, catalytic activity significantly increased in the order of: S-ZrSBA15(26.6) < S-ZrSBA15(15.5) < S-ZrSBA15(5.6) < S-ZrSBA15(10.7), demonstrating that sulfate anions ( $\text{SO}_4^{2-}$ ) act as main active sites for this reaction. Interestingly, this order is not simply consistent with the order of sulfur content or the amount of acid sites, implying a possibility of other factors dominating the catalytic activity. In fact, S-ZrSBA15(26.6) afforded an activity (58.3% after 24 h) far superior to that of the conventional

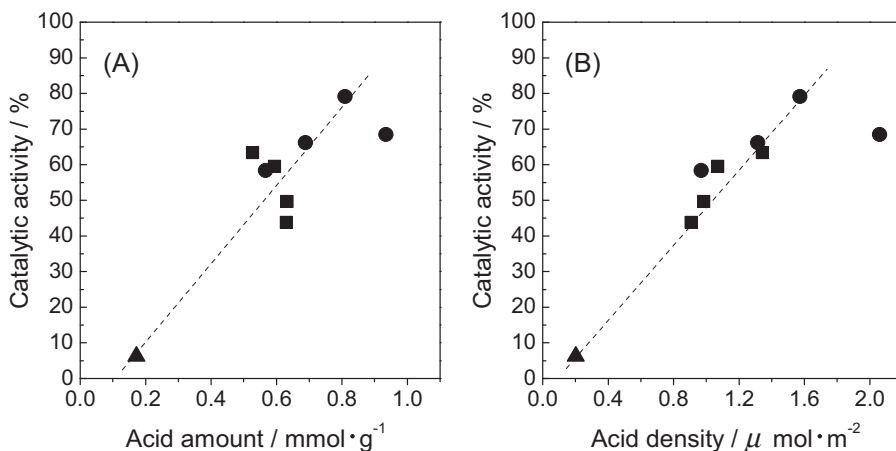


**Fig. 9.** (A) Correlation between catalytic activity and acid amount and (B) correlation between catalytic activity and acid density over sulfated mesoporous zirconosilicate catalysts: (●) S-ZrSBA15 samples, (■) S-mesoZS samples and (▲) unmodified SBA-15.

sulfated zirconia without mesoporosity (31.8% after 24 h), while these two samples possess almost similar acid amounts of 0.567 and 0.534 mmol-NH<sub>3</sub>/g, respectively (see Table 2). Although S-ZrSBA15(5.6) showed the highest acid amount (0.935 mmol-NH<sub>3</sub>/g), its activity was lower than that of S-ZrSBA15(10.7) bearing a smaller amount of acid sites (0.810 mmol-NH<sub>3</sub>/g). Improved catalytic activities were also observed over a series of S-mesoZS catalysts, albeit to a lesser extent in comparison with a series of S-ZrSBA15 catalysts (cf. Fig. 8A and B), where a higher activity was obtained basically as increasing the Zr content. Among the solid acid catalysts examined in this study, S-ZrSBA15 with modest Zr content, S-ZrSBA15(10.7), was found to be the most effective catalyst, affording 79.0% yield of ethyl levulinate at 70 °C after 24 h of reaction.

To elucidate what is the most dominant factor controlling the reaction rate, a quantitative study was performed by plotting the obtained catalytic activities as a function of the amount of the acid sites (Fig. 9A) or as a function of the acid density of the catalysts (Fig. 9B), the latter is defined as the amount of chemisorbed NH<sub>3</sub> per unit of surface area. As shown in Fig. 9A and B it was found that the reaction rate in the esterification of levulinic acid correlates better with the density of acid sites, rather than the amount of acid sites (neither the specific surface area nor the total pore volume provided any reasonable correlations against the activity). As an outlying case, S-ZrSBA15(5.6) deviated from this linear correlation, which is probably due to its subpar pore characteristics (see Table 1), indicating that the ordered mesoporous structure is essential for achieving a high catalytic efficiency. The conventional sulfated zirconia without porous structure largely deviated from the correlation as well (plots are not shown). Considering these facts, it is presumable that dispersibility of the acid sites and the associated accessibility of the organic reactants play an important role in determining the overall activity [36]. It is believed that the mesoporosity-derived large surface area allows the acid sites (mainly SO<sub>4</sub><sup>2-</sup> sites) to be highly dispersed on a solid surface and also enlarges the reaction interface, and thus most of the acid sites become accessible by reactants and catalytically active. Furthermore, this analysis also demonstrated that post-sulfation route is more effective way for achieving high acid density (direct-sulfation route results in the formation of intra-framework SO<sub>4</sub><sup>2-</sup> species) and that the catalytic activity does not so much rely on the crystalline structure of the incorporated Zr species.

### 3.5. Reusability of catalyst

In addition to the catalytic activities, reusability and stability of the catalyst are of key importance for practical applications, because such a biomass conversion reaction is supposed to be operated in a large scale, thereby the lifetime of the catalysts strongly affects the cost of the overall process.

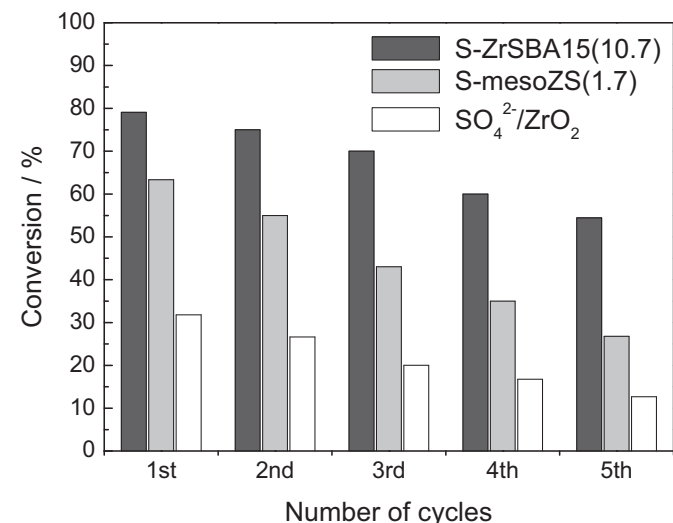
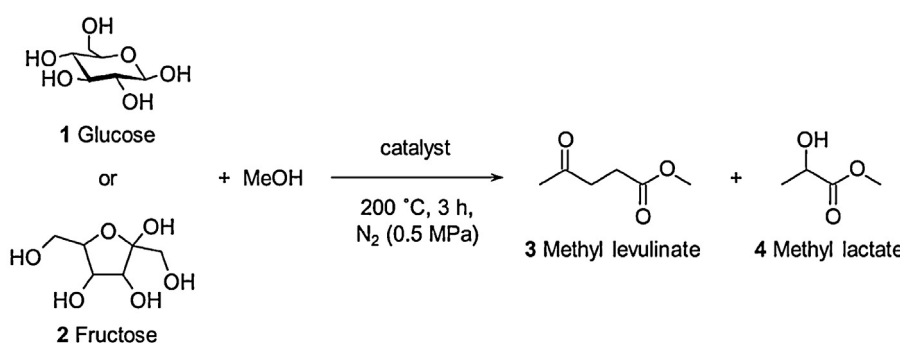


Fig. 10. Catalytic activity of S-ZrSBA15(10.7), S-mesoZS(1.7) and SO<sub>4</sub><sup>2-</sup>/ZrO<sub>2</sub> over 5 repeated cycles in the levulinic acid esterification (5.0 wt% of catalyst, LA:EtOH = 1:10, 70 °C, 24 h, 700 rpm).

To examine the reusability of the catalyst, several selected catalysts were subjected to multiple catalytic cycles under the standard reaction conditions (i.e., 5.0 wt% of catalyst, LA:EtOH = 1:10, 70 °C, 24 h). After each catalytic run, the catalyst had been recovered by filtration, washed with acetone and then calcined at 600 °C in air for 3 h, thereby discounting the possibility of catalyst deactivation by the strongly adsorbed organic species. Fig. 10 compares catalytic activities of S-ZrSBA15(10.7), S-mesoZS(1.7) and the conventional sulfated zirconia over five repeated cycles. As can be seen in Fig. 10, all the catalysts showed a continual activity reduction during moderate cycling; for example, S-mesoZS(1.7) and the conventional sulfated zirconia eventually lost 58% and 60% of their initial activities, respectively, after five catalytic cycles. This considerable activity reduction can primarily be attributed to the substantial loss of acid sites during their repeated use, which is caused by elution of sulfate anions (SO<sub>4</sub><sup>2-</sup>) into the alcohol media (for detailed reaction profiles, see parts A and B). In fact, the sulfur content in S-mesoZS(1.7) decreased from 0.37 to 0.31 wt%, and that in the conventional sulfated zirconia decreased from 0.60 to 0.44 wt% after five repeated use. It needs to be addressed that the activity reduction is not solely attributed to the loss of sulfate anions, but is also attributed to the structural change of the catalyst. Nitrogen adsorption-desorption measurement of the spent catalyst revealed that the BET surface area of the conventional sulfated zirconia decreased from 52 to 29 m<sup>2</sup>/g. This may be the secondary cause of the continual activity reduction, because the reduced surface area restricts the reaction interface, thereby some of the active



Scheme 2. Synthesis of methyl levulinate from glucose and fructose.

acid sites become inaccessible by reactants. On the other hand, S-ZrSBA15(10.7) catalyst lost only 31% of its initial activity after the same number of cycles, demonstrating its superior reusability. This difference in the catalyst durability might be the consequence of the different chemical environment of Zr species; i.e., the monodispersed Zr species incorporated within the silica matrix may have an ability to strongly stabilize the sulfate anions, whereas the crystalline  $ZrO_2$  binds the sulfate anions more weakly.

Additionally, structural analysis of the used zirconosilicate catalysts confirmed that they are crystallographically unchanged without any appreciable porosity reductions even after five repeated catalytic cycles (for XRD patterns and  $N_2$  adsorption isotherms of the spent catalysts, see parts C and D, respectively). Regarding the stability of mesoporous zirconosilicate materials, a number of publications have commonly described that they are thermally/hydrothermally more stable than a pure siliceous analogue [37–39]. These facts indicate that the sulfated mesoporous zirconosilicates, especially the sulfated Zr-SBA-15, can potentially be used as more efficient, reusable and stable solid acid catalysts for the levulinic acid esterification compared to the conventional sulfated zirconia. Although a leaching of some fractions of sulfate anions is likely unavoidable under the reaction conditions applied, it may be successful to retain the initial activity by re-sulfating the catalyst before its reuse.

### 3.6. Direct conversion of sugars over sulfated mesoporous zirconosilicates

Among the conversion technologies for biomass resources, direct conversion of lignocellulosic biomass, such as cellulose, glucose and fructose, into levulinic esters in alcohol media using acid catalysts is one of the most attractive approaches ever reported. The advantages of this conversion pathway are; a high yield of product compared to the reaction in aqueous media, minimized water generation and easy isolation of the product by distillation [31,40–43].

To expand the availability of the sulfated mesoporous zirconosilicate catalysts, a selected sample, S-mesoZS(1.7), was applied to the above reaction to directly synthesize levulinic esters, and was compared to the conventional sulfated zirconia. The reaction was performed in a stainless steel autoclave reactor using 2.5 wt% of catalyst and methanol as an alcohol medium at 200 °C under 0.5 MPa pressure of nitrogen (Scheme 2). The results of the reactions and some related properties of the catalysts are summarized in Table 3. More than 99% conversions of sugars were obtained after 3 h of reaction at 200 °C in each case, indicating that the acidities of the catalysts are strong enough to catalyze monosaccharides. Over the conventional sulfated zirconia, 50.9% and 66.4% methyl levulinic yields were obtained from glucose and fructose, respectively. It should be noted that methyl lactate, a side reaction product, was scarcely formed under the conditions examined in this study, but an equivalent mole of methyl formate, a cleaved counterpart of methyl levulinic, was produced as a byproduct of methyl levulinic [31,40–43]. The remaining fraction of yields is considered to be the carbonaceous species deposited on the catalyst (such as insoluble polysaccharides and humin compounds), otherwise, the intermediate species such as methyl-D-glucopyranoside [43]. Unexpectedly, the sulfated mesoporous zirconosilicate, S-mesoZS(1.7), provided a quite lower methyl levulinic yield compared to the conventional sulfated zirconia under the same reaction conditions, while these two catalysts having almost similar amount of acid sites (0.527 and 0.534 mmol-NH<sub>3</sub>/g, respectively). S-mesoZS(1.7) transformed glucose and fructose into methyl levulinic in 4.7% and 33.3% yield, respectively, suggesting that major part of sugars were deposited on the catalyst surface. This result can be attributed to the mesoporous structure with 2D

**Table 3**  
Direct synthesis of methyl levulinic from glucose and fructose over sulfated zirconia and S-mesoZS(1.7) at 200 °C<sup>a</sup>.

Catalyst	Sulfur content <sup>b</sup> (wt%)	$S_{BET}$ <sup>c</sup> ( $m^2/g$ )	$V_{total}$ <sup>d</sup> ( $cm^3/g$ )	Acidity <sup>e</sup> (mmol/g)	Glucose <sup>f</sup>	Fructose <sup>f</sup>		
						Conversion of 1 (%)	Yield of 3 (%)	Conversion of 2 (%)
$SO_4^{2-}/ZrO_2$	0.60	52	0.08	0.534	>99	50.9	2.6	>99
S-mesoZS(1.7)	0.37	392	0.72	0.527	>99	4.7	trace	>99

<sup>a</sup> Reaction conditions: catalyst (2.5 wt%), sugars (2.5 mmol), 450 mg, MeOH (20 mL), 200 °C, N<sub>2</sub> (0.5 MPa), 3 h.

<sup>b</sup> Determined by the combination of ICP and EDX analyses.

<sup>c</sup> Specific surface area calculated by BET method.

<sup>d</sup> Total pore volume at  $P/P_0 = 0.99$ .

<sup>e</sup> Calculated from NH<sub>3</sub>-TPD profiles.

<sup>f</sup> An equivalent mole of methyl formate was produced as a byproduct of methyl levulinic. The remaining fraction of yields may be the carbonaceous species deposited on the catalyst.

straight pore channels of S-mesoZS(1.7), in which the monosaccharide molecules are considered to be easily condensed and acid-polymerized to form polysaccharides or humin compounds. The thus formed carbonaceous species cause a contamination and block the pore channels, and thus result in the low methyl levulinate yields. The above catalytic experiments demonstrated that a sulfated mesoporous zirconiosilicate is not as suitable catalyst as the conventional sulfated zirconia for direct conversion of sugars into levulinic esters due to the significant deposition of carbonaceous species inside the pores, whereas it effectively works as a solid acid catalyst in the levulinic acid esterification, allowing the high dispersion of acid sites and facilitating the access of the organic reactants.

#### 4. Conclusions

A series of sulfated zirconiosilicates having  $P6mm$  hexagonal mesoporous structure with varied Zr content were synthesized by sol-gel process and via a post-sulfation or via a direct-sulfation procedure, and were applied to the esterification of levulinic acid with ethanol to produce ethyl levulinate. A distinct correlation was observed between the catalytic activity and the density of acid sites, although less ordered porous solids deviated from this correction, showing that dispersibility of the acid sites and the associated accessibility of the organic reactants play an important role in determining the overall activity. Among the catalysts examined, sulfated Zr-SBA-15 with modest Zr content (Si/Zr ratio of 10.7), prepared via a post-sulfation procedure, was found to be the most promising catalysts combining a high catalytic efficiency, recyclability and stability, which far outperformed those of the conventional sulfated zirconia. Recyclability tests demonstrated that the catalysts suffer from the elution of sulfate anions into the alcohol media, and thus cause a continual activity reduction during their repeated use. It was demonstrated that the sulfated mesoporous zirconiosilicates are potential solid acid catalysts for the production of levulinic esters from levulinic acid and alcohols, but further optimization and improvement of the catalytic performance are clearly needed for the advanced application in direct conversion of cellulosic sugars into levulinic esters.

#### Acknowledgements

This work was financially supported by the Grant-in-Aid awarded to Y.K. from the Institute of Advanced Industrial Science and Technology (AIST).

#### Appendix A. Supplementary data

Supplementary data associated with this article can be found, in the online version, at <http://dx.doi.org/10.1016/j.cattod.2013.11.008>.

#### References

- [1] A. Corma, S. Iborra, A. Velty, *Chem. Rev.* 107 (2007) 2411–2502.
- [2] J.N. Chheda, G.W. Huber, J.A. Dumesic, *Angew. Chem. Int. Ed.* 46 (2007) 7164–7183.
- [3] A.A. Peterson, F. Vogel, R.P. Lachance, M. Fröling, M.J. Antal Jr., J.W. Tester, *Energy Environ. Sci.* 1 (2008) 32–65.
- [4] J. Zakzeski, P.C.A. Bruijninckx, A.L. Jongerius, B.M. Weckhuysen, *Chem. Rev.* 110 (2010) 3552–3599.
- [5] F.M.A. Geilen, B. Engendahl, A. Harwardt, W. Marquardt, J. Klankermayer, W. Leitner, *Angew. Chem. Int. Ed.* 49 (2010) 5510–5514.
- [6] J.-P. Lange, R. Price, P.M. Ayoub, J. Louis, L. Petrus, L. Clarke, H. Gosselink, *Angew. Chem. Int. Ed.* 49 (2010) 4479–4483.
- [7] D.J. Braden, C.A. Henao, J. Heltzel, C.C. Maravelias, J.A. Dumesic, *Green Chem.* 13 (2011) 1755–1765.
- [8] M. Vasiliu, K. Guynn, D.A. Dixon, *J. Phys. Chem. C* 115 (2011) 15686–15702.
- [9] J.C. Serrano-Ruiz, A. Pineda, A.M. Balu, R. Luque, J.M. Campelo, A.A. Romero, J.M. Ramos-Fernández, *Catal. Today* 195 (2012) 162–168.
- [10] J. Zhang, S. Wu, B. Li, H. Zhang, *ChemCatChem* 4 (2012) 1230–1237.
- [11] J. Hegner, K.C. Pereira, B. DeBoef, B.L. Lucht, *Tetrahedron Lett.* 51 (2010) 2356–2358.
- [12] Z. Wu, S. Ge, C. Ren, M. Zhang, A. Yip, C. Xu, *Green Chem.* 14 (2012) 3336–3343.
- [13] T. Runge, C. Zhang, *Ind. Eng. Chem. Res.* 51 (2012) 3265–3270.
- [14] G. Pasquale, P. Vázquez, G. Romanelli, G. Baronetti, *Catal. Commun.* 18 (2012) 115–120.
- [15] S. Dharne, V.V. Bokade, *J. Nat. Gas Chem.* 20 (2011) 18–24.
- [16] D.R. Fernandes, A.S. Rocha, E.F. Mai, C.J.A. Mota, V. Teixeira da Silva, *Appl. Catal., A* 425–426 (2012) 199–204.
- [17] Z.-P. Yan, L. Lin, S. Liu, *Energy Fuels* 23 (2009) 3853–3858.
- [18] X.-L. Du, L. He, S. Zhao, Y.-M. Liu, Y. Cao, H.-Y. He, K.-N. Fan, *Angew. Chem. Int. Ed.* 50 (2011) 7815–7819.
- [19] J.M. Tukacs, D. Király, A. Strádi, G. Novodarszki, Z. Eke, G. Dibó, T. Kégl, L.T. Mika, *Green Chem.* 14 (2012) 2057–2065.
- [20] W.R.H. Wright, R. Palkovits, *ChemSusChem* 5 (2012) 1657–1667.
- [21] J.C. Serrano-Ruiz, D. Wang, J.A. Dumesic, *Green Chem.* 12 (2010) 574–577.
- [22] K. Li, J. Hu, W. Li, F. Ma, L. Xu, Y. Guo, *J. Mater. Chem.* 19 (2009) 8628–8638.
- [23] S. Van de Vyver, J. Geboers, S. Helsen, F. Yu, J. Thomas, M. Smet, W. Dehaen, B.F. Sels, *Chem. Commun.* 48 (2012) 3497–3499.
- [24] X.-R. Chen, Y.-H. Ju, C.-Y. Mou, *J. Phys. Chem. C* 111 (2007) 18731–18737.
- [25] L. Fuxiang, Y. Feng, L. Yongli, L. Ruifeng, X. Kechang, *Microporous Mesoporous Mater.* 101 (2007) 250–255.
- [26] S.-Y. Chen, L.-Y. Jang, S. Cheng, *Chem. Mater.* 16 (2004) 4174–4180.
- [27] B.L. Newalkar, J. Olanrewaju, S. Komarneni, *J. Phys. Chem. B* 105 (2001) 8356–8360.
- [28] S.-Y. Chen, J.-F. Lee, S. Cheng, *J. Catal.* 270 (2010) 196–205.
- [29] G.D. Yadav, J.J. Nair, *Microporous Mesoporous Mater.* 33 (1999) 1–48.
- [30] M.L. Grecea, A.C. Dimian, S. Tanase, V. Subbiah, G. Rothenberg, *Catal. Sci. Technol.* 2 (2012) 1500–1506.
- [31] K. Tominaga, A. Mori, Y. Fukushima, S. Shimada, K. Sato, *Green Chem.* 13 (2011) 810–812.
- [32] D.-M. Do, S. Jaenicke, G.-K. Chuah, *Catal. Sci. Technol.* 2 (2012) 1417–1424.
- [33] Y. Kuwahara, D.-Y. Kang, J.R. Copeland, N.A. Brunelli, S.A. Didas, P. Bollini, C. Sievers, T. Kamegawa, H. Yamashita, C.W. Jones, *J. Am. Chem. Soc.* 134 (2012) 10757–10760.
- [34] Y. Kuwahara, D.-Y. Kang, J.R. Copeland, P. Bollini, C. Sievers, T. Kamegawa, H. Yamashita, C.W. Jones, *Chem.—Eur. J.* 18 (2012) 16649–16664.
- [35] B. Tyagi, K.B. Sidhpuria, B. Shaik, R.V. Jasra, *J. Porous Mater.* 17 (2009) 699–709.
- [36] J. Iglesias, M.D. Gracia, R. Luque, A.A. Romero, J.A. Melero, *ChemCatChem* 4 (2012) 379–386.
- [37] Y. Du, S. Liu, Y. Zhang, F. Nawaz, Y. Ji, F.-S. Xiao, *Microporous Mesoporous Mater.* 121 (2009) 185–193.
- [38] A.V. Ivanov, S.V. Lysenko, S.V. Baranova, A.V. Sungurov, T.N. Zangelov, E.A. Karakhanov, *Microporous Mesoporous Mater.* 91 (2006) 254–260.
- [39] J.-M. Liu, S.-J. Liao, G.-D. Jiang, X.-L. Zhang, L. Petrik, *Microporous Mesoporous Mater.* 95 (2006) 306–311.
- [40] L. Peng, L. Lin, J. Zhang, J. Shi, S. Liu, *Appl. Catal. A* 397 (2011) 259–265.
- [41] X. Hu, C.-Z. Li, *Green Chem.* 13 (2011) 1676–1679.
- [42] M. Mascal, E.B. Nikitin, *ChemSusChem* 3 (2010) 1349–1351.
- [43] S. Saravanamurugan, A. Riisager, *Catal. Commun.* 17 (2012) 71–75.